D13

N79-20043

13

IMPROVEMENTS IN SURFACE SINGULARITY ANALYSIS AND DESIGN METHODS

Dean R. Bristow
McDonnell Aircraft Company
McDonnell Douglas Corporation

SUMMARY

The coupling of the combined source-vortex distribution of Green's potential flow function with contemporary numerical techniques is shown to provide accurate, efficient, and stable solutions to subsonic inviscid analysis and design problems for multi-element airfoils. The analysis problem is solved by direct calculation of the surface singularity distribution required to satisfy the flow tangency boundary condition. The design or inverse problem is solved by an iteration process. In this process, the geometry and the associated pressure distribution are iterated until the pressure distribution most nearly corresponding to the prescribed design distribution is obtained. Typically, five iteration cycles are required for convergence. A description of the analysis and design method is presented, along with supporting examples.

INTRODUCTION

The surface panel method philosophy for solving arbitrary incompressible potential flow problems involves the mating of classical potential theory with contemporary numerical techniques. Classical theory is used to reduce an arbitrary flow problem to a surface integral equation relating boundary conditions to an unknown singularity distribution (Reference 1).The contemporary numerical techniques are then used to calculate an approximate solution to the integral equation (References 2-14).

All properly formulated surface panel methods are exact in the sense that the difference between the approximate numerical solution and the exact solution to the integral equation can be made arbitrarily small at the expense of increasing the number of computations. This does not imply that all panel methods are equally successful. Indeed, vast differences exist with respect to prediction accuracy versus computational effort, reliability, simplicity, and applicability to an inverse solution mode for design problems.

The major distinguishing characteristics of panel methods are depicted in Figure 1. For the special case of two-dimensional flow, nearly all the possible combinations of Figure 1 have been formulated and tested at McDonnell Aircraft Company (MCAIR). The most successful of the tested formulations was selected as the foundation for the MCAIR Multi-Element Airfoil Analysis and Design Computer Program, herein after designated the MCAIR Airfoil Program. The analysis (direct) mode calculates the velocity distribution of an arbitrary airfoil geometry, whereas the design (inverse) mode iterates to generate the geometry most nearly corresponding to a prescribed surface velocity distribution. Unusually rapid and consistent convergence is obtained because the inverse algorithm includes all the first order terms in the relationship between arbitrary geometry and velocity perturbations.

This paper presents background theory, the formulation, and representative numerical solutions for the MCAIR Airfoil Program.

NOMENCLATURE

c_ℓ	Airfoil lift coefficient
c_p	Pressure coefficient $[1 - (\frac{V}{V_\infty})^2]$
$\vec{n}$	Unit normal vector to a boundary
$\vec{V}$	Flow velocity
γ	Vortex density
μ	Doublet density
σ	Source Density

SUBSCRIPTS

E	External (fluid) side of a boundary
I	Internal side of a boundary
N	Normal component
T	Tangential component
∞	Free stream conditions

SURFACE SINGULARITY THEORY

Any three-dimensional, incompressible, potential flow field can be considered to be induced by a suitable distribution of source and doublet singularity densities on flow boundary surfaces (Reference 1). It is usually convenient to treat the flow field as the sum of a uniform free stream $\vec{V}_\infty$ plus a disturbance potential field associated with the presence of the body (Figure 2). Then the total velocity $\vec{V}$ at any field point can be expressed as

$$\vec{V} = \vec{V}_\infty + \vec{\nabla}\phi \tag{1}$$

where ϕ is the potential of the disturbance field.

The value of ϕ at an arbitrary field point P can be expressed in the following form:

$$\phi = \frac{1}{4\pi} \iint \left\{ -\frac{\sigma}{r} + \mu \frac{\partial}{\partial n} \left(\frac{1}{r}\right) \right\} ds \qquad (2)$$

where ds is a differential area element at arbitrary surface point Q of the body; r is the distance to point P; n is the distance measured along an axis normal to the body surface at Q, positive outward; and σ and μ are functions of location on the body surface, i.e., functions of Q. σ and μ are respectively the source and doublet densities.

For two-dimensional flow, it is generally more convenient to use vortex singularities in place of doublets. As is proved in Reference 4, a surface doublet distribution of density μ can be replaced by an equivalent vortex distribution where the vortex density vector $\vec{\gamma}$ satisfies the following equation at each surface point:

$$\vec{\gamma} = \vec{n} \times \vec{\nabla}\mu \qquad (3)$$

$\vec{n}$ is the local unit normal vector pointing into the flow field.

It is noteworthy that there is no limit to the number of different solution source - vortex distributions corresponding to any given flow field. The theoretical distinction between the different distributions is best illustrated by examining the imaginary flow field internal to the boundaries (Figure 3). Consider two-dimensional flow. The discontinuity across any surface sheet of sources and vortices can be expressed as follows:

$$V_{N_E} - V_{N_I} = \sigma \qquad (4)$$

$$V_{T_E} - V_{T_I} = \gamma \qquad (5)$$

where σ and γ are the local source and vortex densities. For solid body boundary conditions ($V_{N_E} = 0$), Equation (4) indicates that a vortex-only solution will correspond to $V_{N_I} = 0$ at every internal boundary point. The unique internal flow field generated by zero normal velocity boundary conditions is, of course, stagnation. Then Equation (5) indicates that $V_{T_E} = \gamma$ everywhere on the external surface.

A particularly useful combined source-vortex distribution corresponds to the uniform internal flow field $\vec{V}_I = \vec{V}_\infty$. For this case, Equations (4) and (5) imply that the source and vortex densities are equal to the external perturbation velocity components, i.e.,

$$V_N = V_{N_\infty} + \sigma \qquad (6)$$

$$V_T = V_{T_\infty} + \gamma \qquad (7)$$

Subscript E has been omitted for brevity. The above combined source-vortex distribution is equivalent to the application of Green's third identity (Reference 15) to the perturbation potential ϕ. A schematic of Equations (6) and (7) is presented in Figure 4.

An illustration of the nature of three different singularity distributions corresponding to the same potential field is presented in Figure 5. The theoretical singularity distributions for a source solution, vortex solution, and the combined Green's identity source-vortex solution are shown for the flow around an infinite circular cylinder with flow tangency boundary conditions. It is interesting that the combined source-vortex distribution is a fifty percent blend of the source only and vortex only solutions. Green's identity typically provides a source distribution more mild than the source only solution and a vortex distribution more mild than the vortex only solution.

The combined source-vortex distribution of Green's identity is especially suitable for application to a numerical panel method. The equality between singularity densities and disturbance flow velocity means that regardless of either boundary conditions or geometry, the singularity magnitudes cannot become disproportionately large. This contrasts sharply with source only solutions, for which the source density can increase without bounds as body thickness approaches zero even though the velocity remains finite everywhere. The practical significance is that the mild source-vortex distributions associated with Green's identity eliminate excessive velocity gradients between boundary condition control points, thereby reducing the possibility of leakage. The relationships between disturbance flow velocity and singularity density holds regardless of boundary conditions, be they Neumann, Dirichlet, or mixed. These relationships can always be used to eliminate half the unknown singularity densities a priori, leaving no more effective unknowns that a source only or vortex only approach.

TWO-DIMENSIONAL SOLUTION FORMULATION

The present formulation is based on the combined source-vortex distribution of Green's identity (Equations 6 and 7). Low order panel modeling is employed to the effect that source gradient and surface curvature corrections on each panel are ignored. However, the use of internal potential boundary conditions and the application of the velocity - singularity strength equality results in close to higher order prediction accuracy for most practical geometric shapes. The advantage of the low order modeling is the simplicity inherent in establishing inverse capability.

The geometry of each airfoil element is simulated by a closed polygon, where the polygon segment end points are assumed to lie on the actual airfoil. The midpoint of each segment (panel) is selected as the boundary condition control point.

For Neumann prescribed normal velocity boundary conditions, the source density distribution is established a priori from Equation (6). It is assumed that the source density is uniform on each panel.

The gist of the solution to analysis problems is to determine the appropriate vortex distribution. The vortex density is assumed to vary linearly on each panel and to be continuous at panel end points, with one exception. If the geometry has any slope discontinuities such as a sharp trailing edge, the vortex density is allowed to be discontinuous at the corresponding panel end point. This is consistent with exact theoretical solutions, for which

corners are reflected as discontinuities in the vortex distribution. The magnitude of the discontinuity is an additional unknown which is determined through the introduction of an internal boundary condition control point near the corner. The distance from the corner is nominally selected as 1% of the local panel length.

Instead of directly imposing prescribed normal velocity boundary conditions at the control points, a theoretically equivalent approach first applied by Morino, et al (Reference 13) is used. Consistent with the internal velocity field $\vec{V}_I = \vec{V}_\infty$, uniform internal perturbation potential is prescribed at each control point of an airfoil element. In the present two-dimensional formulation, this is easily accomplished by specifying that the analytical line integral of perturbation velocity component along an internal path connecting adjacent control points be zero.

The circulation of each airfoil element is controlled by either of two methods at the discretion of the user. First, the net vortex strength can be prescribed directly. Alternately, a Kutta condition can be applied in which the velocity normal to the trailing edge bisector is set equal to zero at a location approximately 2% local segment length downstream. The nominal 2% value has been selected because it consistently provides lift coefficient prediction accuracy that agrees within 1% of the virtually exact conformal solution of Catherall et al. (Reference 16) for typical panel models.

Imposition of the potential boundary conditions and one circulation control equation per airfoil element establishes a system of linear equations with the same number of unknown vortex densities as equations. This number is equal to the sum of the total number of panels and total number of sharp corners. Solution to the system renders the complete set of singularities known.

At each control point, the surface velocity is calculated from Equation (7) and, for steady state flow, the pressure distribution is calculated by Bernoulli's equation

$$c_p = 1 - \left(\frac{V_T}{V_\infty}\right)^2 - \left(\frac{V_N}{V_\infty}\right)^2 \qquad (8)$$

Force and moment integration is performed under the assumption that the control point pressure applies uniformly to each panel.

Inverse solutions are generated in accordance with the iterative-linearization philosophy developed in Reference 17. For the elements to be designed in a multi-element airfoil system, the following steps are involved:

(1) The user prescribes a design pressure or velocity distribution around the surfaces of the various elements.

(2) The user prescribes a starting geometry to initialize the calculations and the location of one point per element to be fixed in space, such as the trailing edge.

(3) The program solves the direct problem for the geometry, in order to determine the change in velocity distribution required to achieve the prescribed values.

(4) The program calculates the rate of change of surface velocity with respect to an arbitrary change in surface angle distribution. Each element perimeter remains fixed. If the tangential component of velocity at the control point of the ith panel is designated V_{T_i} and if the surface angle of the jth panel is designated θ_j, then the array A_{ij} is calculated where

$$A_{ij} = \frac{\partial V_{T_i}}{\partial \theta_j}$$

(5) The change in surface angle distribution is calculated in accordance with the prescribed velocities and the following first order expression:

$$\Delta V_{T_i} \tilde{=} \sum_j (A_{ij} \Delta\theta_j)$$

(6) The geometry is corrected by the program and steps (3)- (5) are repeated as a series of iteration cycles.

The most difficult and important step in formulating the inverse capability is to generate the matrix A_{ij}. It is noted that all terms were incorporated in deriving the partial derivative, including singularity strength changes and the displacement of panels j+1, j+2, etc. corresponding to the surface angle change $d\theta_j$. The corresponding singularity strength changes are obtained by a first order expansion to the boundary condition equation. In order to obtain numerical stability in the inverse process, the velocities are prescribed not only at the panel midpoints but at endpoints as well. Then the solution involves minimizing the mean square error between the prescribed and calculated distributions.

EXAMPLE SOLUTIONS

The following examples demonstrate the numerical behavior of the present MCAIR Airfoil Program as compared to alternate approaches.

The benefits of using a combined source-vortex distribution versus source-only is improved accuracy for (1) thin highly loaded airfoils and for (2) sharp concave corners. Examples of the former are presented in Reference 14 and are not repeated here. The latter is typical of wing-fuselage intersections and is represented by the wedge-cylinder example of Figure 6. Both

the present method and the Douglas Neumann source method (Reference 2) were applied to the geometry using identical panel modeling (244 panels). The results are virtually identical except near the sharp concave corner, in which region the source solution diverges while the present solution properly approaches stagnation.

The advantage of the internal potential boundary conditions is reflected in the calculated pressure distribution for the Karman-Trefftz airfoil of Figure 7. In each of the three calculated panel method distributions, the combined source-vortex distribution of Green's identity was applied and the exact lift coefficient from the Catherall-Sells solution was prescribed. Converting from the direct imposition of zero normal velocity boundary conditions to prescribed internal perturbation potential generates the same type of accuracy improvement as obtained by applying higher order corrections for source gradient and panel curvature effects. For each of the three panel method solutions, the conversion from calculated singularity density to surface velocity was conducted by the most accurate approach, namely, Equation (7) for potential boundary conditions and the summation of influence coefficients for flow tangency.

The third example demonstrates prediction accuracy of the MCAIR method for one of the few two-element airfoils for which an exact conformal mapping solution is available for comparison (Reference 18). Using a total of 66 panels, the geometry and calculated pressure distributions at zero incidence are presented in Figure 8. The agreement with the exact solution is good, including the calculated lift corresponding to the trailing edge bisector Kutta condition.

The objective of the first inverse example is to design a circular cylinder by the MCAIR method using a nearly flat plate for the starting geometry (Figure 9). The exact analytical surface velocity distribution was prescribed, and the converged solution geometry of Figure 9 was obtained after four iteration cycles. The panel endpoints are within a maximum distance of 0.002 radius of lying on a circle. The complete partial derivatives of velocity with respect to surface angle change were necessary but not sufficient for obtaining convergence about the periphery of this example. The use of mild combined source-vortex singularites is also a factor. To illustrate, the example was repeated, but this time vortex-only singularities were used to induce the flow field in accordance with the analysis method of Dvorak and Woodward (Reference 7). The geometry never converged (Figure 10) but oscillated $\pm 30^{o}$ in the leading edge region from one iteration cycle to the next.

The final example demonstrates inverse solution capability for the two-element Williams airfoil presented earlier in Figure 8. The starting geometry of Figure 11 was used to initialize the calculations, and the calculated surface velocity distribution of Figure 8 was prescribed on both elements. The geometry converged and agreed with the target geometry to within a tolerance of one-tenth of one degree in five iterations (Figure 11).

The above examples are typical of the accuracy and numerical stability of the MCAIR Airfoil Program. On the CDC CYBER 173, a two-element airfoil

analysis solution using 70 panels total requires approximately 4 seconds computing time. For the corresponding inverse solution, approximately 20 seconds is required per iteration cycle.

CONCLUDING REMARKS

The use of the source-vortex distribution of Green's identity coupled with internal perturbation potential boundary conditions provides a simple, accurate, reliable, and efficient procedure for solving airfoil incompressible potential flow problems. For a wide range of geometric shapes, low order paneling modeling generates prediction accuracy usually associated with higher order solutions. The procedure is especially suitable for application to inverse design problems.

REFERENCES

1. Lamb, Sir Horace, Hydrodynamics, 6th Edition, Cambridge University Press, 1932.

2. Hess, J.L. and Smith, A.M.O., "Calculation of Potential Flow About Arbitrary Bodies," Progress in Aeronautical Sciences, Vol. 8, Pergamon Press, New York, 1966.

3. Hess, J.L., "Higher-Order Numerical Solution of the Integral Equation for the Two-Dimensional Neumann Problem," Computer Methods in Applied Mechanics and Engineering, Vol. 2, No. 1, February 1973.

4. Hess, J.L., "Calculation of Potential Flow about Arbitrary Three-Dimensional Lifting Bodies," MDC Report J5679-01, October 1972.

5. Martensen, E., "Berechnung der Druckverteilung an Gitterprofilen in Ebener Potentialstromung mit einer Fredholmschen Integralgleichung," Archive for Rational Mechanics and Analysis, Vol. 3, No. 3, 1959.

6. Oellers, H.J., "Die Inkompressible Potentialstromung in der Ebener Gitterstuffe," Jahrbuch 1962 der Wissenschaftlichen Gesellschaft fur Luft-und Raumfahrt, pp. 349-353.

7. Dvorak, F.A., and Woodward, F.A., "A Viscous/Potential Flow Interaction Analysis Method for Multi-Element Infinite Swept Wings," NASA CR-2476, November 1974.

8. Stevens, W.A., Goradia, S.H., and Braden, J.A., "Mathematical Model for Two-Dimensional Multi-Component Airfoils in Viscous Flow," NASA CR-1843, July 1971.

9. Halsey, N.D., "Methods for the Design and Analysis of Jet-Flapped Airfoils," AIAA Paper No. 74-188, February 1974.

10. Maskew, B., "A Subvortex Technique for the Close Approach to a Discretized Vortex Sheet," Vortex-Lattice Utilization Workshop, NASA Langley Research Center, May 1976.

11. Tulinius, J.R., "Theoretical Prediction of Thick Wing and Pylon-Fuselage-Fanpod-Nacelle Aerodynamic Characteristics at Subcritical Speeds," NASA CR137578, July 1974.

12. Johnson, F.T., and Rubbert, P.E., "Advanced Panel-Type Influence Coefficient Methods Applied to Subsonic Flows," AIAA Paper 75-50, January 1975.

13. Chen, L.T., Suciu, E.O., and Morino, L., "A Finite Element Method for Potential Aerodynamics Around Complex Configurations," AIAA Paper 74-107, January 1974.

14. Bristow, D.R., "Recent Improvements in Surface Singularity Methods for the Flow Field Analysis About Two-Dimensional Airfoils," AIAA Paper 77-641, June 1977.

15. Kellogg, O.D., Foundations of Potential Theory, Dover Publications, Inc., New York, 1953, p. 219.

16. Catherall, D., Foster, D.N., and Sells, C.C.L., "Two Dimensional Incompressible Flow Past a Lifting Aerofoil," R.A.E. TR-69118, 1969.

17. Bristow, D.R., "A New Surface Singularity Method for Multi-Element Airfoil Analysis and Design," AIAA Paper 76-20, January 1976.

18. Williams, B.R., "An Exact Test Case for the Plane Potential Flow About Two Adjacent Lifting Aerofoils," Aeronautical Research Council R&M No. 3717, September 1971.

TABLE 1.- MODIFICATIONS OF THE SUBROUTINES IN THE BASELINE VERSION

Subroutine	No change	Minor change	Major change	Delete
MAIN			X	
POINT	X			
SLOPE	X			
TRANS			X	
DISTP	X			
FTLUD				X
DIR	X			
LSQ				X
PROOT	X			
MAIN1			X	
READIT		X		
GEOM			X	
ROTRAN			X	
ASLOT			X	
NORMAL			X	
MAIN 2			X	
CHEN			X	
MATRIX			X	
POTLF			X	
CAMBER				X
SMOOTH	X			
VOVBT				X
THICK				X
COMPR			X	
STAG			X	
MAIN 3			X	
LOAD			X	
LAMNA		X		
BLTRAN		X		
TURBL		X		
TURB		X		
DERIV		X		
START		X		
CONFBL				X
CONF 5				X
CONF 7		X		
CONF 8		X		
DLIM	X			

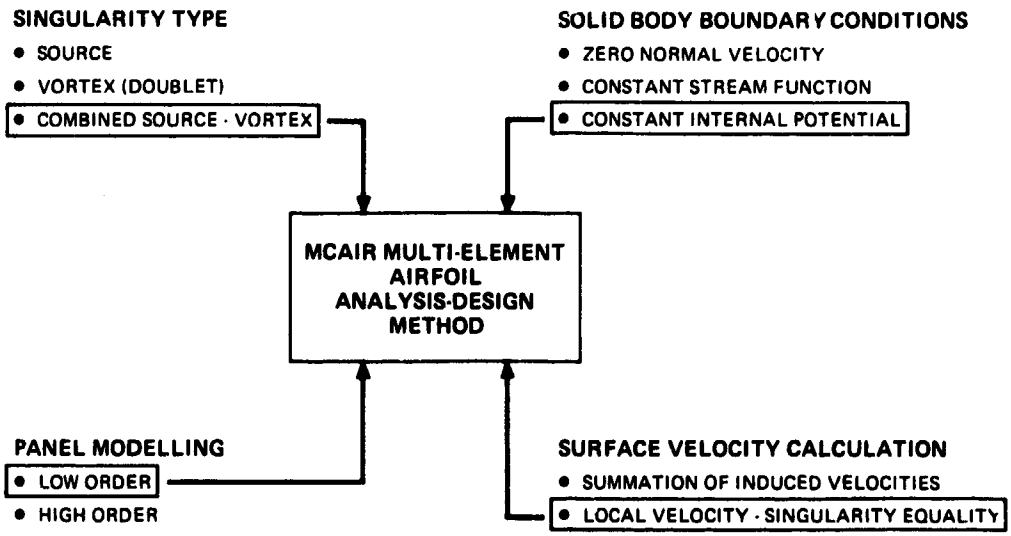

Figure 1.- Diagram of surface singularity panel methods for incompressible, potential flow.

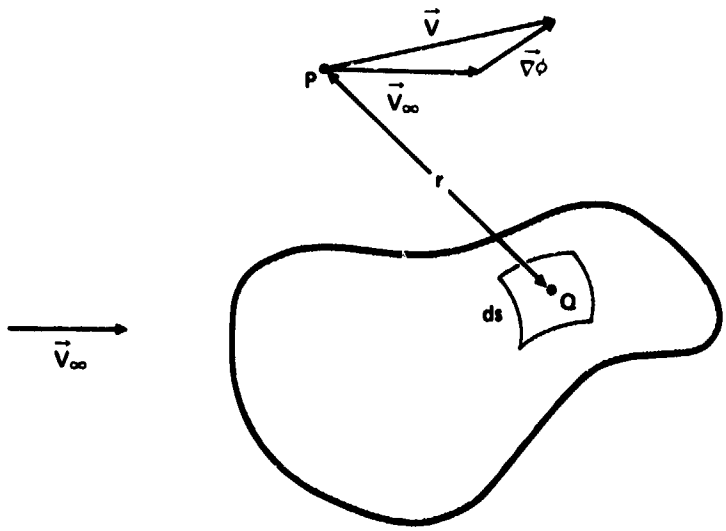

Figure 2.- Body immersed in an unbounded flow field.

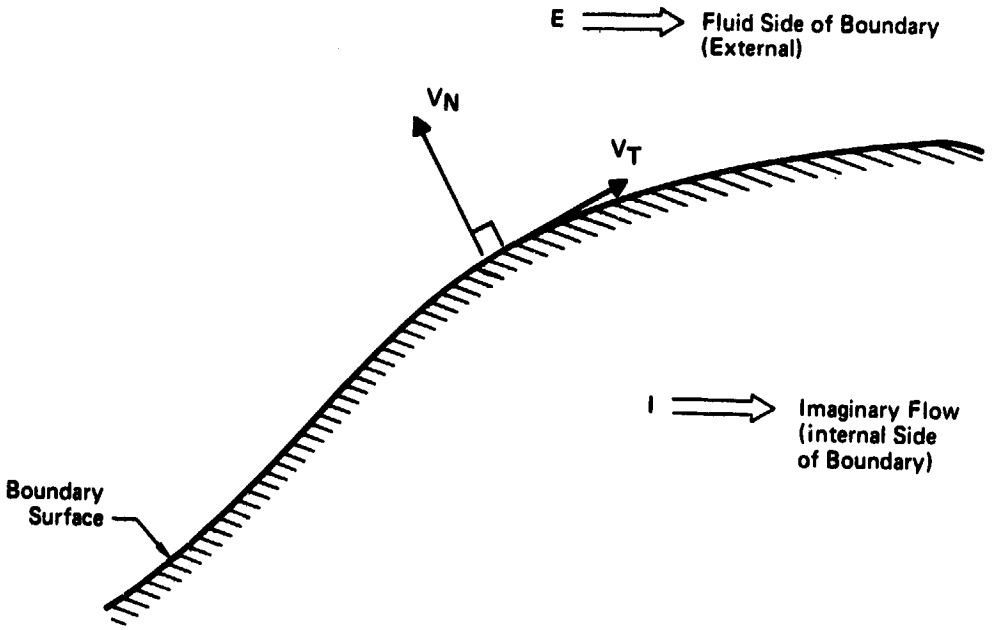

Figure 3.- Two sides of a flow boundary surface.

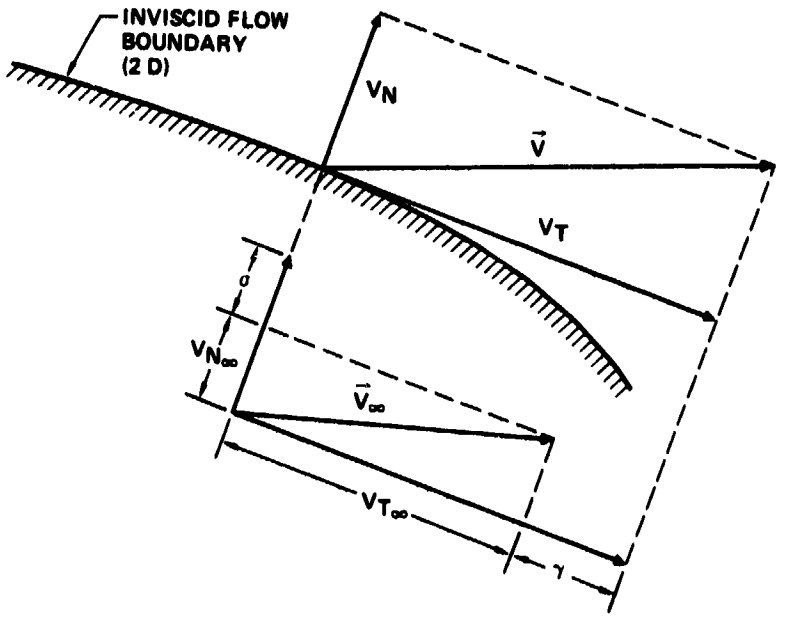

Figure 4.- Green's identity velocity-singularity relationship.

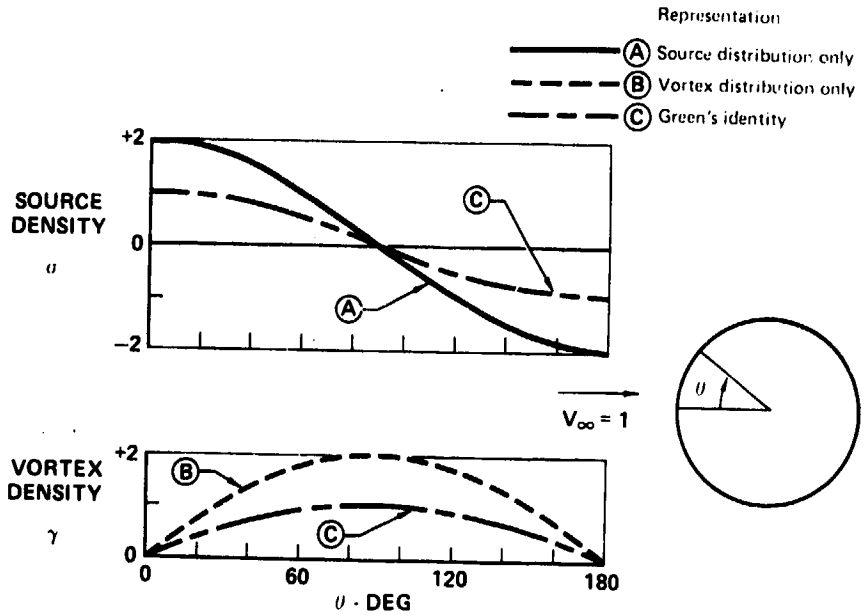

Figure 5.- Equivalent singularity representations for a circular cylinder.

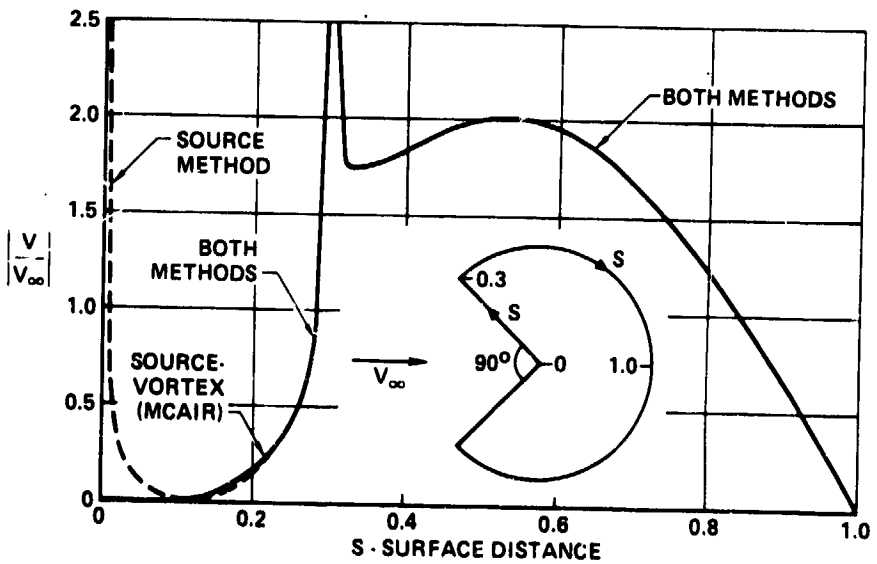

Figure 6.- Comparisons of source and source-vortex solutions. Concave corner flow.

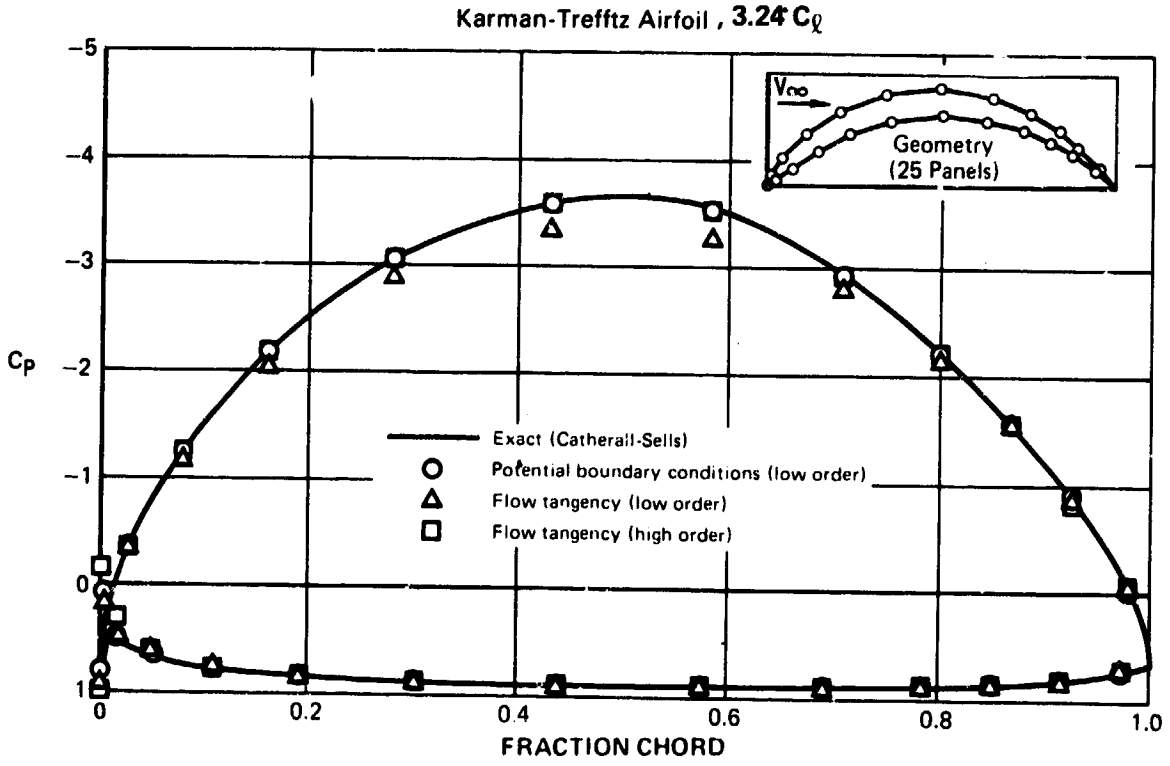

Figure 7.- Effect of panel modeling and boundary conditions.

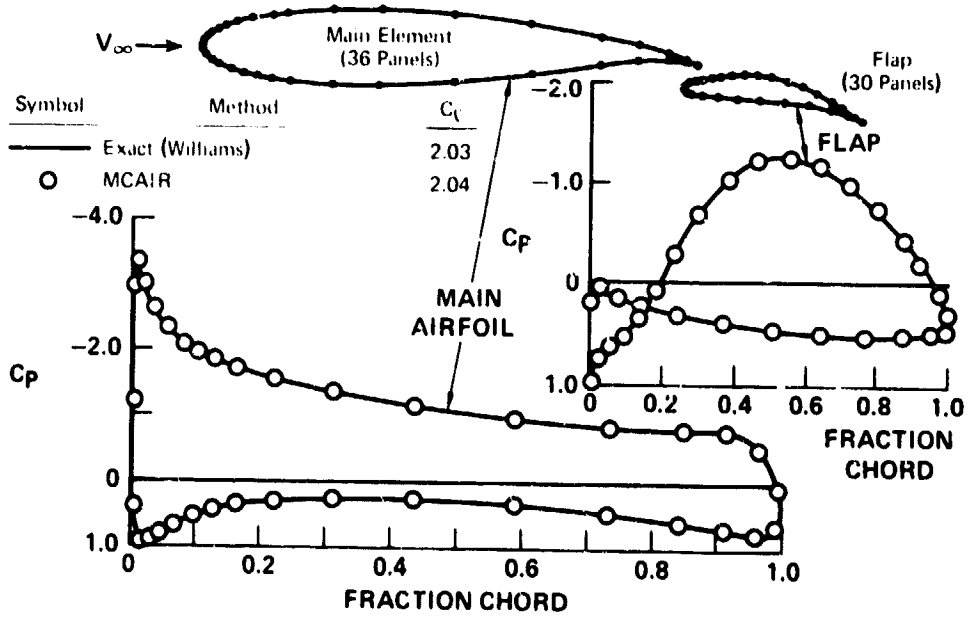

Figure 8.- Two-element airfoil solution. MCAIR method.

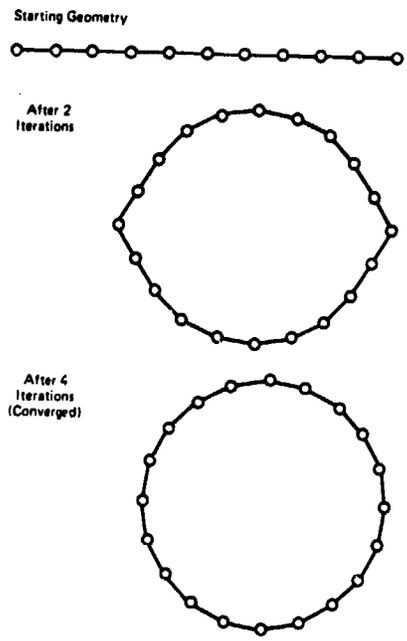

Figure 9.- Circular-cylinder inverse solution. MCAIR method.

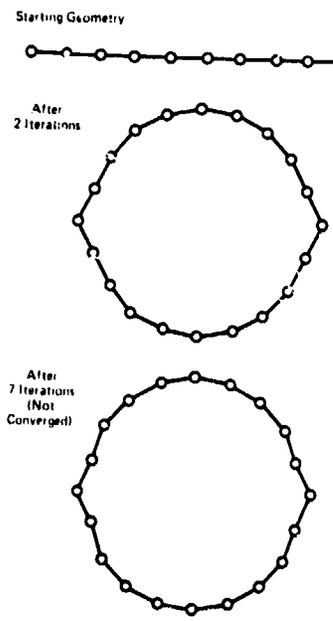

Figure 10.- Circular-cylinder inverse solution.
Vortex-only method.

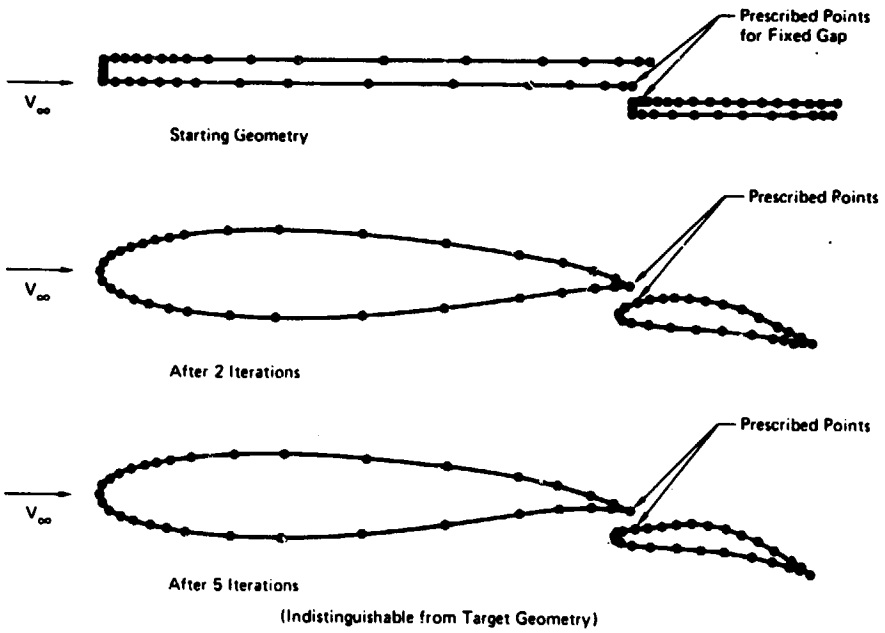

Figure 11.- Two-element airfoil inverse solution.
MCAIR method.